# Atmospheric dynamics and West European summer hot temperatures since 1871

M Carmen Alvarez-Castro, Davide Faranda, Pascal Yiou

# Atmospheric dynamics and West European summer hot temperatures since 1871

**M. Carmen Alvarez-Castro, Davide Faranda, Pascal Yiou**

Laboratoire des Sciences du Climat et de l'Environnement, UMR 8212

CEA-CNRS-UVSQ, IPSL, Université Paris-Saclay, F-91191 Gif-sur-Yvette, France

E-mail: carmen.alvarez-castro@lsce.ipsl.fr

December 2016

**Abstract.** Summer hot temperatures have many impacts on health, economy (agriculture, energy, transports) and ecosystems. In western Europe, the recent summers of 2003 and 2015 were exceptionally warm. Many studies have shown that the genesis of the major heat events of the last decades was linked to anticyclonic atmospheric circulation and to spring precipitation deficit in southern Europe. Such results were obtained for the second part of the 20th century and projections into the 21st century. In this paper, we challenge this vision by investigating the earlier part of the 20th century from an ensemble of 20CR reanalyses. We propose an innovative description of Western-European heat events that takes into account the dynamics of the circulation. We argue that the atmospheric circulation patterns leading to the most intense heat events have changed during the last century. We also show that the increasing temperature trend during major heatwaves is encountered during episodes of Scandinavian blocking, while other circulation patterns do not yield temperature

trends during extremes.

*Keywords*: Weather Regimes, Climate Dynamics, Heat Events

## 1. Introduction:

In western Europe, recent hot summers were characterized by highly anomalous meteorological conditions. In these situations, such as 2003, the heat was prolonged and intense, and the consequences were disastrous for society and ecosystems (Schär & Jendritzky 2004, Robine et al. 2008, Wreford & Adger 2010, Poumadere et al. 2005, Ciais et al. 2005).

European surface temperature variations are influenced by processes that combine radiative forcing, the large-scale atmospheric circulation and local phenomena. Over the last five decades, most of the intense European heat events have been connected to prolonged spells of anticyclonic circulation (Scandinavian blocking) and dry spring conditions in Southern Europe (Schär et al. 1999, Fischer et al. 2007, Mueller & Seneviratne 2012, Zampieri et al. 2009, Quesada et al. 2012, Vautard et al. 2007). However, the Summer 2011 was cool and preceded by a dry spring; the Summer 2013 was warm and preceded by a wet spring; and the Summer 2015 was warm with persisting southerly atmospheric flows and no lasting blocking episodes. The goal of this paper is to assess the robustness of the link between heat events and atmospheric circulation. We perform a statistical and dynamical analysis on a long period that covers 1871–2015. Since anticyclones extend to a radius of few hundreds kilometers, such a connection

must be investigated on a regional scale (Della-Marta et al. 2007, Stefanon et al. 2012). Hence, we restrict our analysis to Western Europe in the region covering France and the Iberian Peninsula, whose weather conditions are strongly influenced by the atmospheric circulation over the North Atlantic. This analysis also puts some of the results of Horton et al. (2015) on this link into a broader time perspective.

## 2. Data and Methods:

We base our analysis on the sea-level pressure (SLP) and the surface temperature fields during summers (June-July-August: JJA) in 20th Century Reanalysis data (20CR: 1871–2011, (Compo et al. 2011)). To ensure the robustness of the results, we used the ensemble mean (EM) and 10 members (M0-M9) of the ensemble. The analysis is completed with other reanalysis products: NCEP (1948–2015) (Kalnay et al. 1996) and ERA20C reanalysis (1900–2000) (Poli et al. 2013) (see supplementary material). In order to describe the variability of the atmospheric circulation, we decompose the summer SLP anomalies field (obtained by removing the seasonal cycle) into four weather regimes following the approach of Yiou et al. (2008) and study their connection with heat events at seasonal(i) and sub-seasonal(ii) timescales in Western-Europe [10°W – 7.5°E; 35 – 50°N]. i) Seasonal: the 20 summers with high mean temperature anomalies of the period 1871–2011, and ii) Subseasonal: heatwaves defined as periods with high temperatures anomalies for at least five consecutive days. In both analyses temperatures are detrended by removing a linear trend calculated from the time series of summer seasonal means.

The goal of the detrending is to remove the effect of the well-documented European temperature increase, which does not depend on the weather pattern.

### *2.1. Weather Regimes:*

Weather regimes are recurring states of the atmospheric circulation and provide a useful description of the atmospheric variability (Michelangeli et al. 1995, Corti et al. 1999). Following the methods of Michelangeli et al. (1995) and Yiou et al. (2008) we compute four weather regimes over the North Atlantic region [80°W – 50°E; 20 – 70°N] (Fig. 1a-d) using the first ten Empirical Orthogonal Functions (EOFs), which calculated on daily NCEP SLP anomalies (reference period: 1970–2010) over the summers (JJA). To weigh the variations of the grid cell surface, the data are normalized by the square root of cosine of latitude. The k-means algorithm (Michelangeli et al. 1995) is applied to the ten first EOFs of the SLP anomalies to compute the four cluster centroids. The Principal Components centroids are recomposed with the EOFs to obtain the weather regimes in physical space. For comparison, we classify different reanalysis datasets with the NCEP weather regimes. All the reanalysis data are interpolated onto the NCEP grid ($2.5° \times 2.5°$). The SLP data classifications of all reanalyses are obtained by determining the minimum of the Euclidean distances to the four NCEP summer weather regime centroids. This is achieved without further EOF truncation. The NCEP summer weather regimes are shown in Fig. 1a-d, with the same nomenclature as in Cassou et al. (2005): a) the negative phase of North Atlantic Oscillation (NAO−) showing a dipole between

Greenland and Northern Europe, b) the Atlantic Ridge (AR), with a high pressure over the center of the North Atlantic and some common features with the positive phase of NAO, c) Scandinavian Blocking (BLO), with a high pressure center over Scandinavia, d) Atlantic Low (AL), with a low pressure center covering the central North Atlantic.

To ensure that there are no inhomogeneities in the method, we have verified that the RMSE between the reference period and the other periods/datasets is small (Fig. S8).

*2.2. Projection onto weather regimes for a dynamical representation:*

In order to visualize the dependence between the daily SLP fields and the four weather regimes, we represent the *trajectory* of each summer in the space of correlations (Fig. 2a-c) using an approach based on dynamical systems theory (Katok & Hasselblatt 1997) . In this framework, the motion of a particle is represented in the space defined by its position and speed (the so-called phase space). In our set-up, the particle is replaced by a SLP field and the directions in phase space correspond to the projections on the four weather regimes. Trajectories provide additional information with respect to the monthly average statistical quantities, on the time dependence and the coherence of the dynamical projection with respect to weather regime bases. If a trajectory jumps every day to a different region of the phase space, then a dominant weather regime is not representative of the dynamical behavior of events lasting several days. If instead

the trajectory occupies a restricted region of the phase space with smooth transitions of the projection among weather regimes, then the dynamical representation is informative and the base of weather regimes is appropriate.

This is equivalent to assuming the existence of a low-dimensional attractor. The caveat is that the weather regime description is a first order simplification of the atmospheric circulation that captures large scale features. Although this phase-space method has been debated since Lorenz (1991), there are theoretical (Chekroun et al. 2011) and experimental (Casdagli et al. 1991) evidences that such a procedure is effective when the dynamics can be projected on a low dimensional phase space with a stochastic perturbation.

## 3. Results and Discussion:

The link between the North Atlantic atmospheric circulation and heat events over France and the Iberian Peninsula is investigated at two timescales.

### *3.1. Seasonal scale: weather regimes during the warmest summers*

We carried out a statistical analysis of the 20 hottest summers of the period 1871–2011 (Fig. 1i). In Western-Europe [10°W – 7.5°E; 35 – 50°N], the 20 hottest summers (Fig. 1i and 2) are defined in each dataset as the ones having the highest average temperature anomalies with respect to the climatology. Figure 1e-h shows the anomalous summer frequency of weather regimes in 20CR with respect to the NCEP reference period. In

this figure we see how NAO- is the unique regime decreasing in frequency with the time, and BLO is the one increasing in frequency with the time. Figure 1i shows the dominant regime as the one with the highest anomalous frequency. We find a general agreement between all the 20CR members and the EM in terms of warmest summers and the dominating weather regime. Most of the warmest summers (largest circles in Fig. 1i) occur during the second part of the 20th century. As observed by Stott et al. (2004) and Meehl & Tebaldi (2004), they also increase in frequency over time. Our analysis shows significant changes in the dominating weather regimes associated with warmest summers. If BLO is dominant from the second part of 20th century, scarce occurrences of this weather regime are found before 1930, even within the ensemble members of 20CR. BLO and AL regimes are conducive to warm extremes and NAO- and AR are the opposite (Cassou et al. 2005). Figure 1i shows that, after 1930, it is more frequent to find hottest summers linked to what we know as warm regimes. BLO (the most frequent one after 1930) leads to stagnant air and potential land-surface feedbacks, whereas AL relies on advection from lower latitudes. In the other hand, NAO$-$ is the dominant weather regime during warmerst summers up to 1930. This weather regime contributes to a weakening of the westerly flow from the Atlantic into Western Europe. AR regime is more stable in time (Figure 1f, 1i).

To understand such trends we decompose the average information found with the statistical analysis via the dynamical representation of the warmest summers, defined in

section 2.2. We project the SLP anomaly fields onto NAO− and AR regimes, which are the most frequent for the first part of the 20th century as shown in Fig. 1 e. This analysis synthesizes the trajectory of the atmospheric circulation during heat events in a space represented by the weather regimes. Consistently with the previous analysis, we find that the atmospheric dynamics has evolved from patterns that are positively correlated with NAO− during the late 19th century (Fig. 2 a), to negative correlations during the rest of the record (Fig. 2 b-c). Similar projections on BLO and AL regimes show: that BLO has the opposite change of NAO-, being negative during the first period (Figure S4a) and positive during the last one (Figure S4c). AR and AL regimes do not show significant differences between the periods. Those correlations add a daily temporal information that is not captured by the analysis of the dominating seasonal weather regime (Figure 1i) and highlight a change of atmospheric behavior. Thus the dominant weather regime is a valid concept as the trajectories of heatwaves persist at sub-seasonal scales around the same region of the phase space. These changes are consistent within the 20CR ensemble, as the M0-M9 average (Fig. 2d) shows consistent results with the EM.

### *3.2. Subseasonal scale: weather regimes during heatwaves events*

To understand whether those results hold also for short time events (at least 5 consecutive days), independently from the fact that they have been observed during hot summers, we compute the average temperature during heatwaves striking Western-

Europe.

Heatwave events are defined when the summer temperature exceeds a threshold /percentiles (P90, P95) for more than 5 consecutive days. Figure 3 shows heatwave events above the P90 threshold, computed on the area temperature anomalies (France and the Iberian Peninsula). Temperatures in figure 3 are average values during each heatwave event. Heatwaves events are grouped by the dominating weather regime. We find that 19% of total events are dominated by NAO− (Fig. 3a), 36%, by BLO (Fig. 3c). Heatwaves that are associated by AR (Fig. 3b) and AL (Fig. 3d) weather regimes have a frequency of 19% and 26%, respectively. Summer heatwave events dominated by BLO regime have an increasing trend of 0.12°C/decade along the period reaching temperatures up to 29 °C in the beginning of the 21st century. We also find that the longest events are associated to BLO regime (Fig. 3e). On the contrary, NAO− have a decreasing trend of −0.06°C/decade reaching 26 °C at the end of the 19th century, and 24 °C in the beginning of the 21st century. BLO is the only one with a significant trend (p-values in Table S2, supplementary material).

To shed more light on the circulaion changes, we compute composites of SLP and surface temperature anomalies for pre-1930 heatwaves (figure 4a) and post-1930 heatwaves (4c) during all the heatwave events found in analysis of figure 3. The exercise is repeated by taking into account the occurrence of NAO− heatwave events for pre-1930 (4b) and the occurrence of BLO heatwave events for post-1930 (4d). The temperature pattern changes in pre and post 1930 maps mainly in Greenland and the East coast

of North America and in Europe. Pressure patterns for all the heatwave events pre and post-1930 reproduce well NAO− and BLO (respectively) albeit weaker for the BLO regime. So, even if there is a change for NAO−, BLO is the one with a stronger change for short-term events, because it is the most representative pattern in heatwaves events from 1930.

## 4. Conclusions:

These results confirm that most heat events (either warmest summers and heatwaves in Western Europe) of the second half of the 20th century occurred when the Scandinavian Blocking weather regime dominated the North Atlantic region, causing increasing temperatures and more frequent and longer heatwaves events (figure 3 and figure S7). Our results also show that NAO− is more favorable to drive warm summers before 1930. This early period corresponds to the most frequent co-occurrence of this regime and heatwaves events. Although the increasing temperature trends observed during blocking heatwaves episodes could be attributed to secular climate change (Coumou et al. 2014), the change in the dominating weather regimes may have a different explanation, e.g. the decadal variability of the atmospheric dynamics. Those findings are consistent with the results of Horton et al. (2015), although we consider heatwaves on a finer spatial scale (Western-Europe).

The robustness of our results is ensured by the use of 20CR ensemble and other reanalysis datasets (see supplementary material). The dynamical analysis also suggests

that there is an increase of negative correlations between warmest summers and the NAO− regime.

Although the information extracted in warmest summers and heatwaves is a priori different, our analysis shows similar results at different timescales. In terms of warmest summers, NAO− was the most representative pattern up to 1930 and from 1930 on, and BLO is the most representative one. For short time heat events, the most representative is BLO during the whole period but, as for warmest summers, NAO- events are less frequent after 1930. BLO is associated to the longest and hottest heatwaves and yields an increasing trend, as outlined by Horton et al. (2015).

In the debate on the mechanisms leading to changes in the atmospheric circulation (Shepherd 2014), our results demonstrate the signature of the impacts of the atmospheric circulation on European heat events.

**Acknowledgments:**

M.C.A-C. was supported by the Swedish Research Council grant No. C0629701 (MILEX). D.F. was supported by the ERC grant No. 338965–A2C2. P.Y. was supported by the European Unions Seventh Framework Programme grant No. 607085–EUCLEIA. The authors thank G. Compo, for the help supported with data from members of 20CR reanalysis. 20CR and NCEP Reanalysis data provided by the NOAA/OAR/ESRL PSD, Boulder, Colorado, USA, from their Web site at http://www.esrl.noaa.gov/psd/. ERA-20C reanalysis data provided by the ECMWF

(European Centre for Medium-Range Weather Forecasts), Reading, UK, from their website at http://apps.ecmwf.int/datasets/data/era20c-daily/.

## Supplementary information:

Available in the online version of the paper. Correspondence and requests for materials should be addressed to M.C.A-C (email: carmen.alvarez-castro@lsce.ipsl.fr).

## References:

Casdagli, M., Eubank, S., Farmer, J. D. & Gibson, J. (1991). State space reconstruction in the presence of noise, *Physica D.* **51**(1): 52–98.

Cassou, C., Terray, L. & Phillips, A. S. (2005). Tropical atlantic influence on European heat waves, *J. Climate* **18**(15): 2805–2811.

Chekroun, M. D., Simonnet, E. & Ghil, M. (2011). Stochastic climate dynamics: Random attractors and time-dependent invariant measures, *Physica D.* **240**(21): 1685–1700.

Ciais, P. et al. (2005). Europe-wide reduction in primary productivity caused by the heat and drought in 2003, *Nature* **437**(7058): 529–533.

Compo, G. P. et al. (2011). The twentieth century reanalysis project, *Q. J. Roy. Meteor. Soc.* **137**(654): 1–28.

Corti, S., Molteni, F. & Palmer, T. (1999). Signature of recent climate change in frequencies of natural atmospheric circulation regimes, *Nature* **398**(6730): 799–802.

Coumou, D., Petoukhov, V., Rahmstorf, S., Petri, S. & Schellnhuber, H. J. (2014). Quasi-resonant circulation regimes and hemispheric synchronization of extreme weather in boreal summer, *Proceedings of the National Academy of Sciences* **111**(34): 12331–12336.

Della-Marta, P. M., Luterbacher, J., von Weissenfluh, H., Xoplaki, E., Brunet, M. & Wanner, H. (2007). Summer heat waves over western Europe 1880–2003, their relationship to large-scale forcings and predictability, *Clim. Dynam.* **29**(2-3): 251–275.

Fischer, E., Seneviratne, S., Lüthi, D. & Schär, C. (2007). Contribution of land-atmosphere coupling to recent European summer heat waves, *Geophys. Res. Lett.* **34**(6).

Horton, D. E., Johnson, N. C., Singh, D., Swain, D. L., Rajaratnam, B. & Diffenbaugh, N. S. (2015). Contribution of changes in atmospheric circulation patterns to extreme temperature trends, *Nature* **522**(7557): 465–469.

Kalnay, E. et al. (1996). The NCEP/NCAR 40-year reanalysis project, *B. AM. Meteorol. Soc.* **77**(3): 437–471.

Katok, A. & Hasselblatt, B. (1997). *Introduction to the modern theory of dynamical systems*, Vol. 54, Cambridge University Press.

Lorenz, E. N. (1991). Dimension of weather and climate attractors, *Nature* **353**(6341): 241–244.

Meehl, G. A. & Tebaldi, C. (2004). More intense, more frequent, and longer lasting heat waves in the 21st century, *Science* **305**(5686): 994–997.

Michelangeli, P.-A., Vautard, R. & Legras, B. (1995). Weather regimes: Recurrence and quasi stationarity, *J. Atmos. Sci.* **52**(8): 1237–1256.

Mueller, B. & Seneviratne, S. I. (2012). Hot days induced by precipitation deficits at the global scale, *Proc. Natl. Acad. Sci.* **109**(31): 12398–12403.

Poli, P. et al. (2013). The data assimilation system and initial performance evaluation of the ecmwf pilot reanalysis of the 20th-century assimilating surface observations only (ERA-20C), *ECMWF ERA Rep* **14**: 59.

Poumadere, M., Mays, C., Le Mer, S. & Blong, R. (2005). The 2003 heat wave in France: dangerous climate change here and now, *Risk Anal.* **25**(6): 1483–1494.

Quesada, B., Vautard, R., Yiou, P., Hirschi, M. & Seneviratne, S. I. (2012). Asymmetric European summer heat predictability from wet and dry southern winters and springs, *Nature Clim. Change*

**2**(10): 736–741.

Robine, J.-M., Cheung, S. L. K., Le Roy, S., Van Oyen, H., Griffiths, C., Michel, J.-P. & Herrmann, F. R. (2008). Death toll exceeded 70,000 in Europe during the summer of 2003, *C. R. Biol.* **331**(2): 171–178.

Schär, C. & Jendritzky, G. (2004). Climate change: hot news from summer 2003, *Nature* **432**(7017): 559–560.

Schär, C., Lüthi, D., Beyerle, U. & Heise, E. (1999). The soil-precipitation feedback: A process study with a regional climate model, *J. Climate* **12**(3): 722–741.

Shepherd, T. G. (2014). Atmospheric circulation as a source of uncertainty in climate change projections, *Nat. Geosci.* **7**(703-708).

Stefanon, M., D'Andrea, F. & Drobinski, P. (2012). Heatwave classification over Europe and the Mediterranean region, *Environ. Res. Lett.* **7**(1): 014023.

Stott, P. A., Stone, D. A. & Allen, M. R. (2004). Human contribution to the European heatwave of 2003, *Nature* **432**(7017): 610–614.

Vautard, R., Yiou, P., D'andrea, F., De Noblet, N., Viovy, N., Cassou, C., Polcher, J., Ciais, P., Kageyama, M. & Fan, Y. (2007). Summertime European heat and drought waves induced by wintertime Mediterranean rainfall deficit, *Geophys. Res. Lett.* **34**(7).

Wreford, A. & Adger, W. N. (2010). Adaptation in agriculture: historic effects of heat waves and droughts on UK agriculture, *Int. J. Agric. Sustain.* **8**(4): 278–289.

Yiou, P. et al. (2008). Weather regime dependence of extreme value statistics for summer temperature and precipitation, *Nonlinear Proc. Geoph.* **15**(3): 365–378.

Zampieri, M., D'Andrea, F., Vautard, R., Ciais, P., de Noblet-Ducoudré, N. & Yiou, P. (2009). Hot European summers and the role of soil moisture in the propagation of mediterranean drought, *J. Climate* **22**(18): 4747–4758.

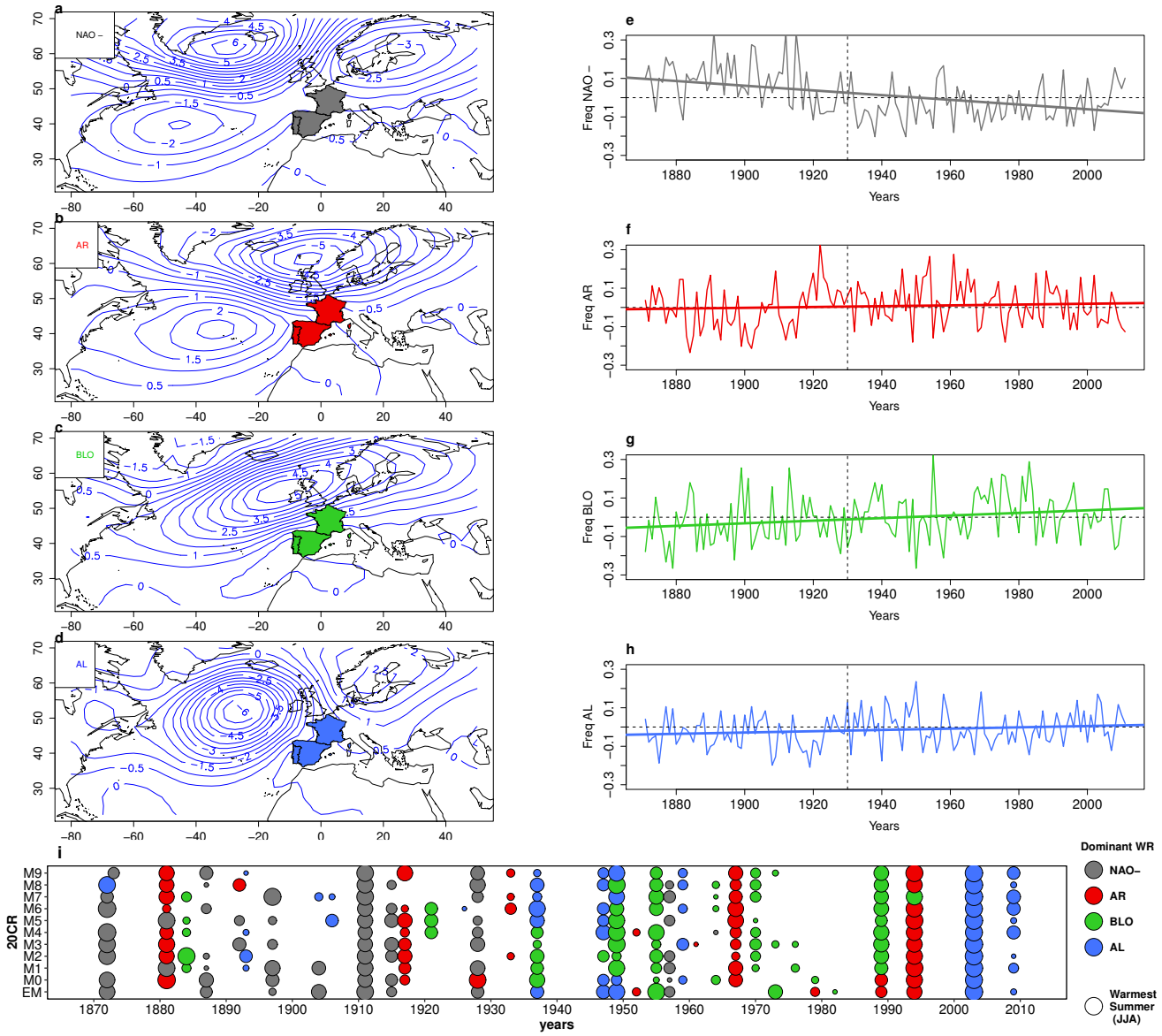


**Figure 1. Summer SLP weather regimes over the North-Atlantic region and their dominance in the twenty warmest summers during 1871-2011 in Western-Europe.** **a-d,** Summer SLP (hPa anomalies) Weather regimes: **a,** North Atlantic Oscillation in its negative phase (NAO−). **b,** Atlantic Ridge (AR). **c,** Blocking (BLO). **d,** Atlantic Low (AL) weather regime. **e-h,** Long-term weather regime frequency (anomalies) with respect the reference period (NCEP 1970-2010)**i,** Twenty warmest summers in Western-Europe (colored region in **a-d**) with their dominant weather regime. Years are shown in $x$ axis, while $y$ axis displays each of the 20CR members (M0 – M9) and the 20CR EM. Circle size depends on temperature (anomalies), the largest the warmest. Colors represents the dominant weather regime for each summer based in the highest anomalous frequency in **e-h**.

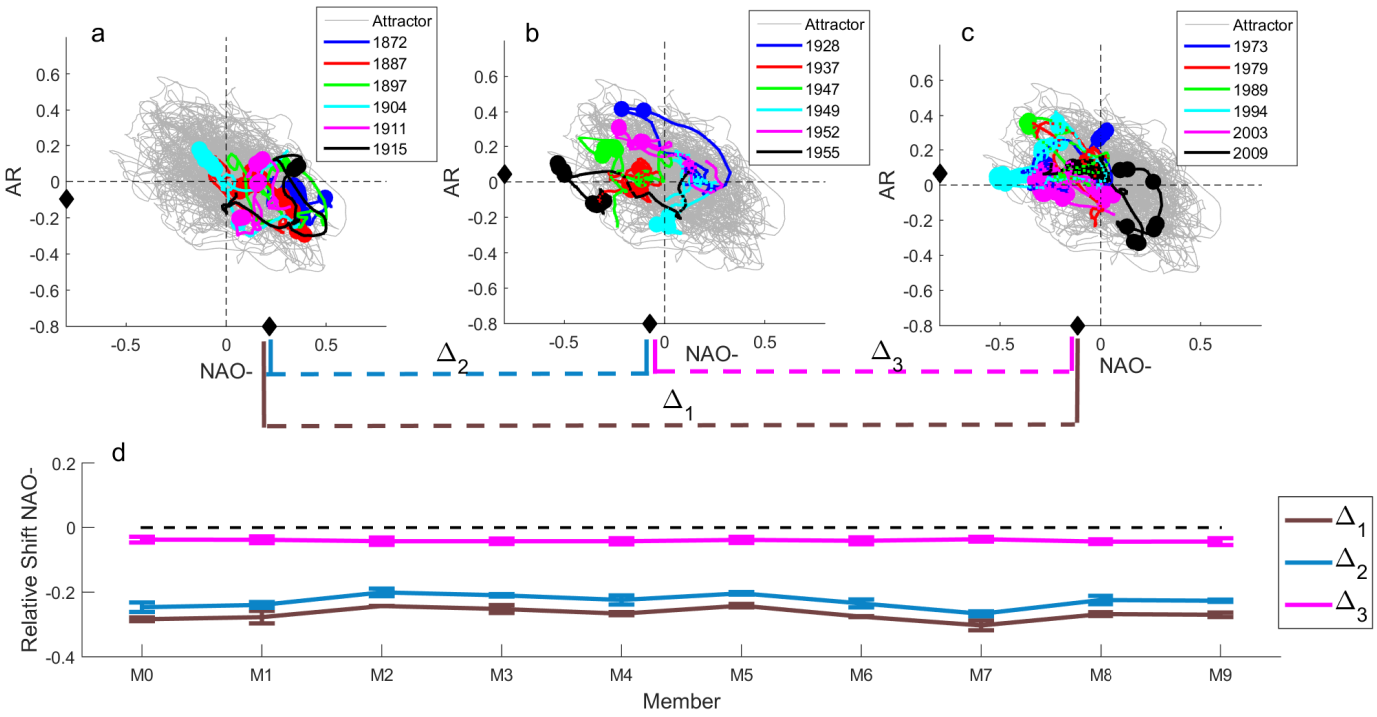


**Figure 2. Dynamical representation of the warmest summers. a-c,** Correlations of daily SLP fields and NAO− ($x$-axis), AR (y-axis) weather regimes for three different periods. Warmest summers are colored as in the legend, light grey lines represent all data. Big circles represent days with temperature above 85th percentile. Average correlations of warmest summers with respect to the NAO− weather regimes (black circle on $x$-axis) and relative difference between the periods ($\Delta 1 - 2 - 3$) for each member of the ensemble (**d**). Errorbars correspond to the standard deviation of the mean. A moving average filter with a 30 day window has been applied to the data.

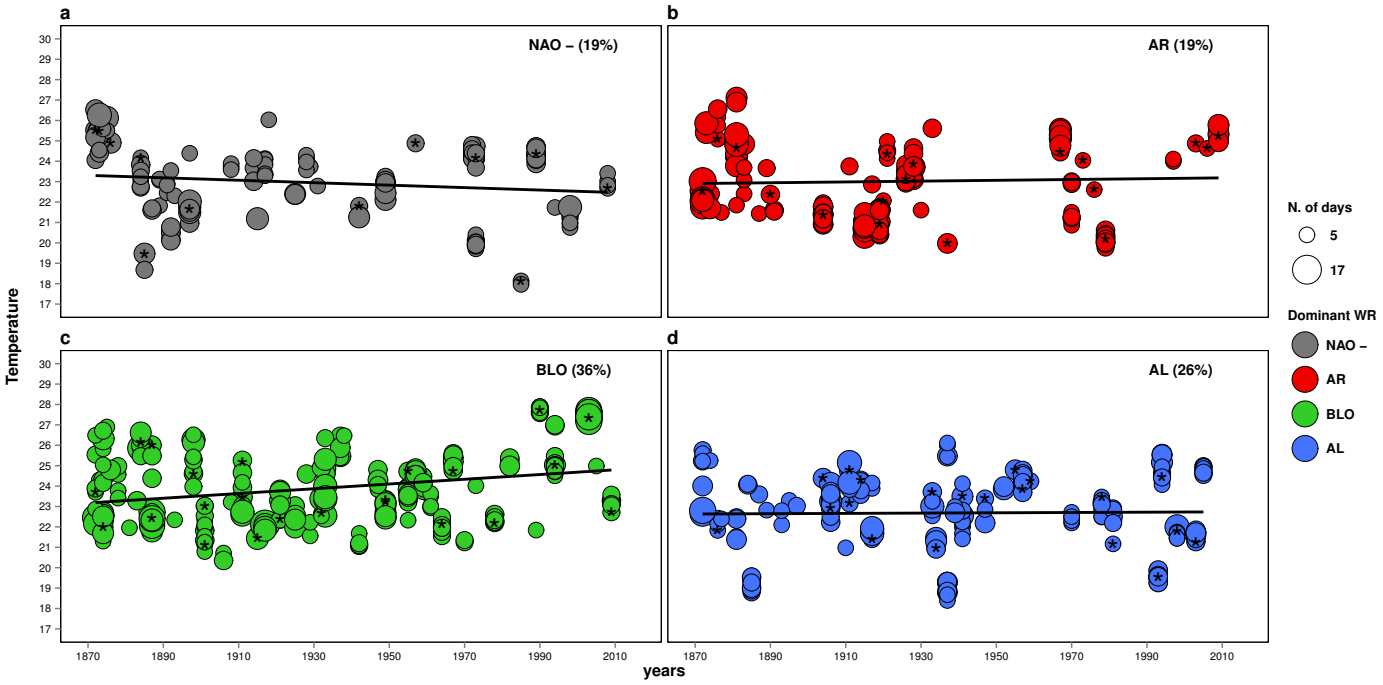


**Figure 3. Dominant weather regimes during Summer heatwave events.** In **a–d,** Summer heatwave events (90th Percentile) for members and EM (circles with stars) of 20CR data, 1871–2011. Colors correspond to the dominant weather regime in each event, temperature ($y$-axis) and years ($x$-axis). Circle sizes depend on the event duration by number of days, the larger the longer duration. Percentages show the frequency of each weather regime. Linear fits are shown in black solid lines.

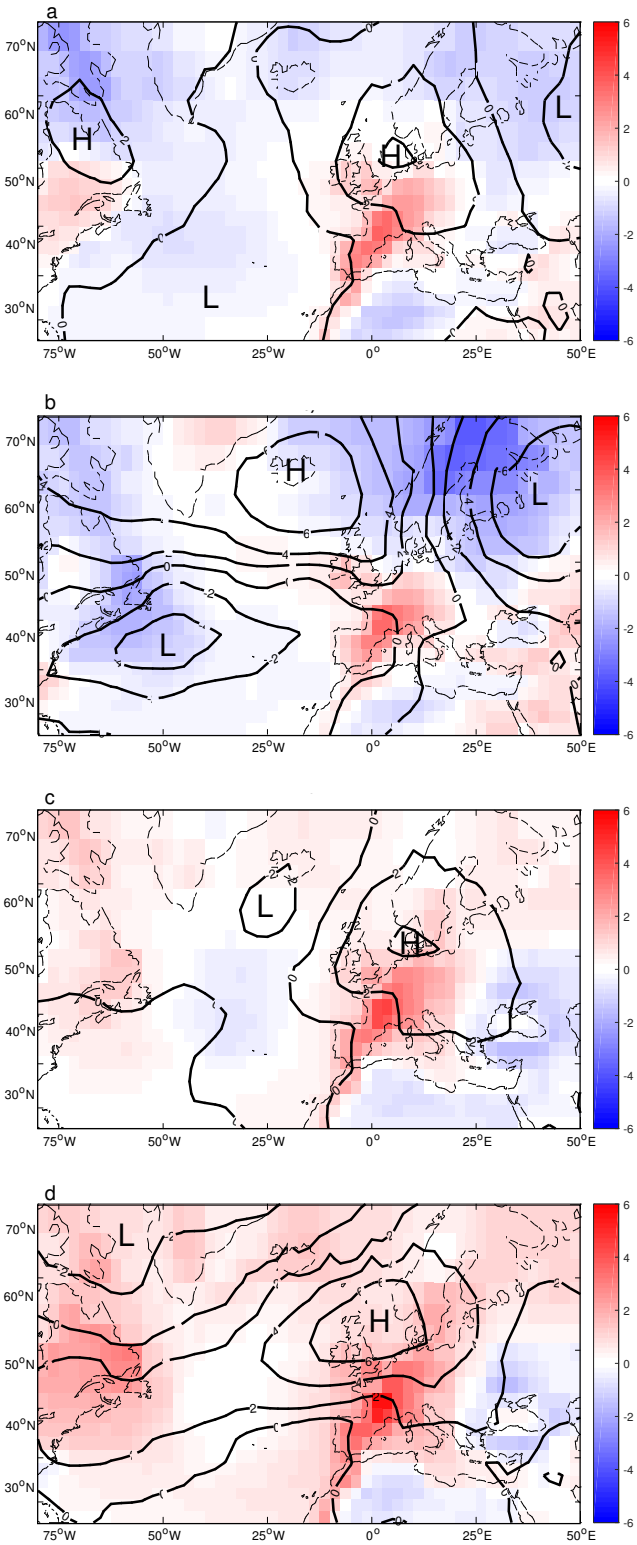


**Figure 4. Composites of Sea Level Pressure (SLP) and Surface Temperature anomalies (SAT) pre/post 1930.** In **a–b,** composites SLP (hPa) and SAT (°C) anomalies for a) all the days during heatwaves events found before 1930, in b) just the events where NAO- was the dominant weather regime. In **c–d,** composites SLP and SAT for c) all days during heatwaves events found after 1930, in d) just the events where BLO was the dominant regime.

# Atmospheric dynamics leading to West European summer hot temperatures since 1871

**M. Carmen Alvarez-Castro, Davide Faranda, Pascal Yiou**

Laboratoire des Sciences du Climat et de l' Environnement, UMR 8212

CEA-CNRS-UVSQ, IPSL, Université Paris-Saclay, F-91191 Gif-sur-Yvette, France

E-mail: carmen.alvarez-castro@lsce.ipsl.fr

December 2016

## Supplementary Material

- Figure S1: Relative long-term summer weather regime frequency over the North-Atlantic region and their dominance in warmest summers in Western-Europe (1871-2015) using three reanalysis products (20CR, ERA20C, NCEP).
- Figure S2: Summer average temperatures for Western-Europe for three reanalysis products (20CR, ERA20C, NCEP).
- Figure S3: Temperature anomalies during warmest summers (IP-France) with dominance of each weather regime in three reanalysis products (20CR, ERA20C, NCEP).
- Figure S4: Dynamical representation of the warmest summers for 20CR Ensemble

mean during 1871-2011 in regimes BLO-AL.

- Figure S5: Dynamical representation of the warmest summers for ERA20C during 1900-2010 in regimes AR-NAO- and BLO-AL.
- Figure S6: Dominants weather regimes during Summer Heatwave events in Western-Europe for three reanalysis products (20CR, ERA20C, NCEP).
- Figure S7: Temperature (y-axis) vs numbers of days (x-axis) during each heatwave event for the 20CR Ensemble Mean (1871-2011) weather regimes.
- Table S1: Absolute root mean square error by period and weather regime.
- Table S2: p-values of Heatwaves events in each dataset.
- Table S3: Average correlations for Fig2 with/without 30-days filter for each regime.

## References


- Chambers, J. M. (1992). Linear models. Chapter 4 of Statistical Models in S eds J. M. Chambers and T. J. Hastie, Wadsworth Brooks/Cole.
- Wilkinson, G. N. and Rogers, C. E. (1973). Symbolic descriptions of factorial models for analysis of variance. *Applied Statistics*, **22**: 3929.

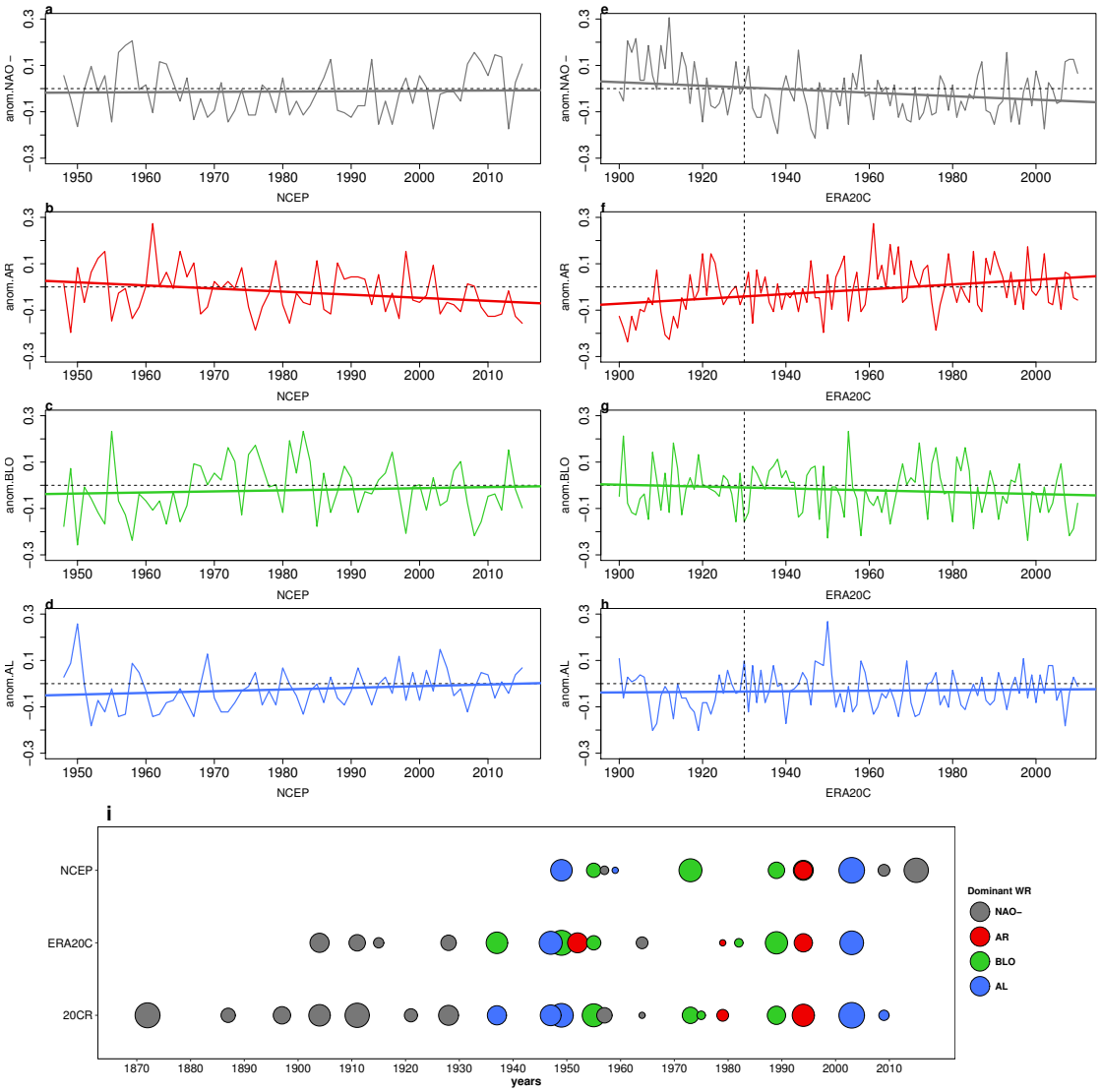


**Figure 1. Relative long-term summer weather regime frequency over the North-Atlantic region and their dominance in warmest summers in Western-Europe (1871-2015) using three reanalysis products (20CR, ERA20C, NCEP)**. As in figure 1, relative frequency of Summer SLP (hPa anomalies) weather regimes: NAO- (**a,e**), AR ( **b,f**), BLO (**c,g**) and AL (**d,h**), but considering NCEP data (**a-d,**) and ERA20C (**e-h**). **e,** Warmest summers from 1871 to 2015 in Western-Europe with their dominant weather regime. Years are shown in x axis while y axis display each of the reanalysis products (20CR, ERA20C, NCEP). Circle size depends on temperature anomalies, the largest the warmest. Colors (black, red, green, blue) represents the dominant weather regime (NAO-, AR, BLO, AL) for each summer. The number of warmest summers are ponderate with the length of each dataset.

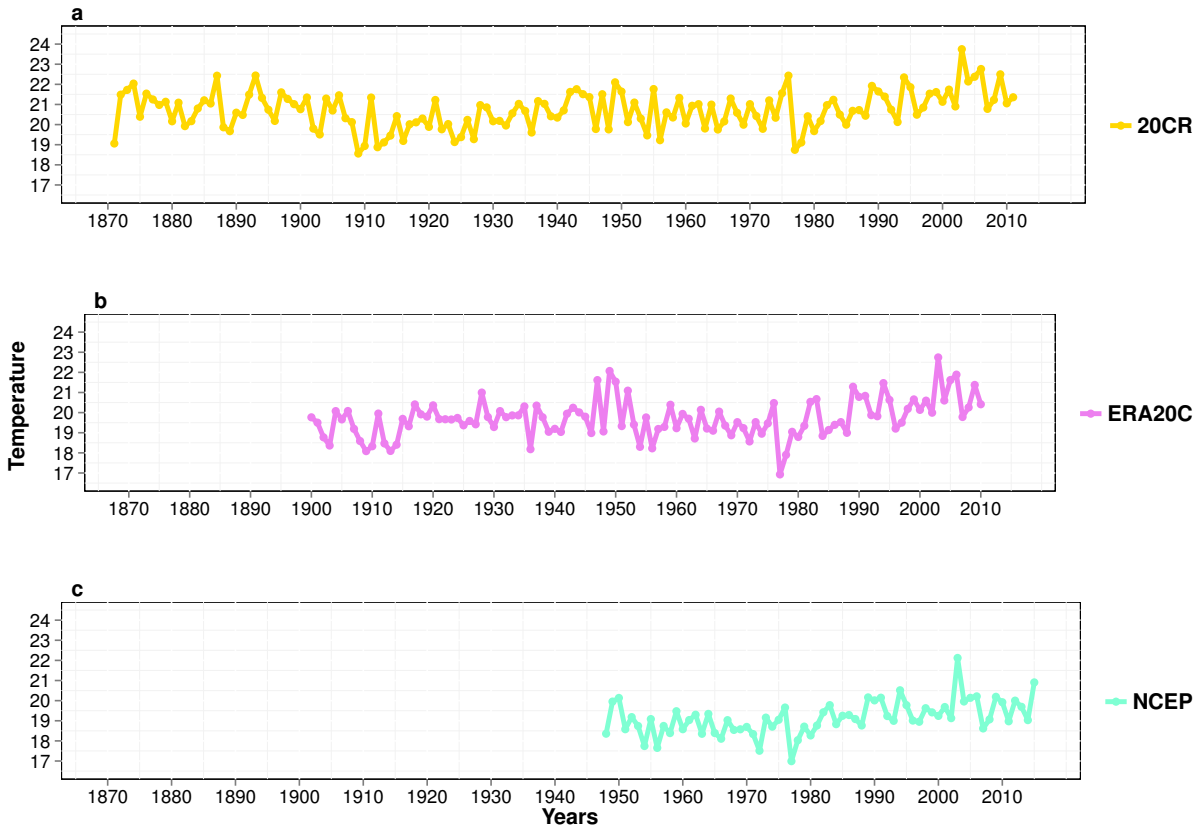


**Figure 2. Summer average temperatures (°C) for Western-Europe. a,** 20CR **b,** ERA20C and **c,** NCEP).

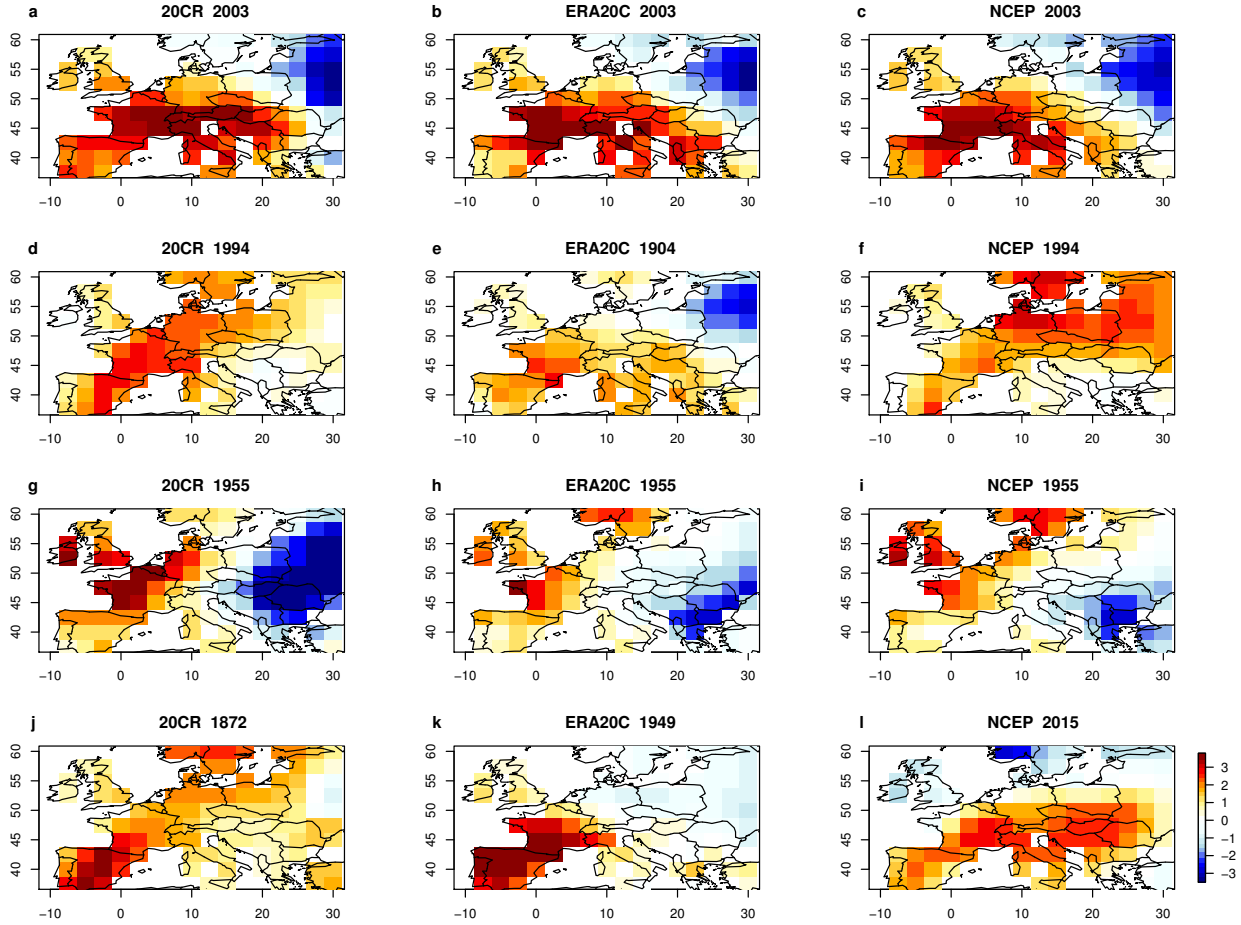


**Figure 3. Temperature anomalies maps for warmest summers in Western-Europe.** Each row correspond to a different dominant weather regime for some explanatory summers. Each column is a different reanalysis product.**a-c,** Summer 2003, where AL was the dominant weather regime. **d-f,** Summer of 1994, where AR was the dominant weather regime (Same frequencies of BLO and AR for NCEP during this summer). **g-i,** Summer of 1955, where BLO was the dominant weather regime. **j-l,** Since there is not a common summer for all the reanalysis datasets with NAO- as a dominant weather regime, here we show the most warmest summer (1872, 1904, 2015) where NAO- was the dominant weather regime in each reanalysis dataset (20CR, ERA20C, NCEP).

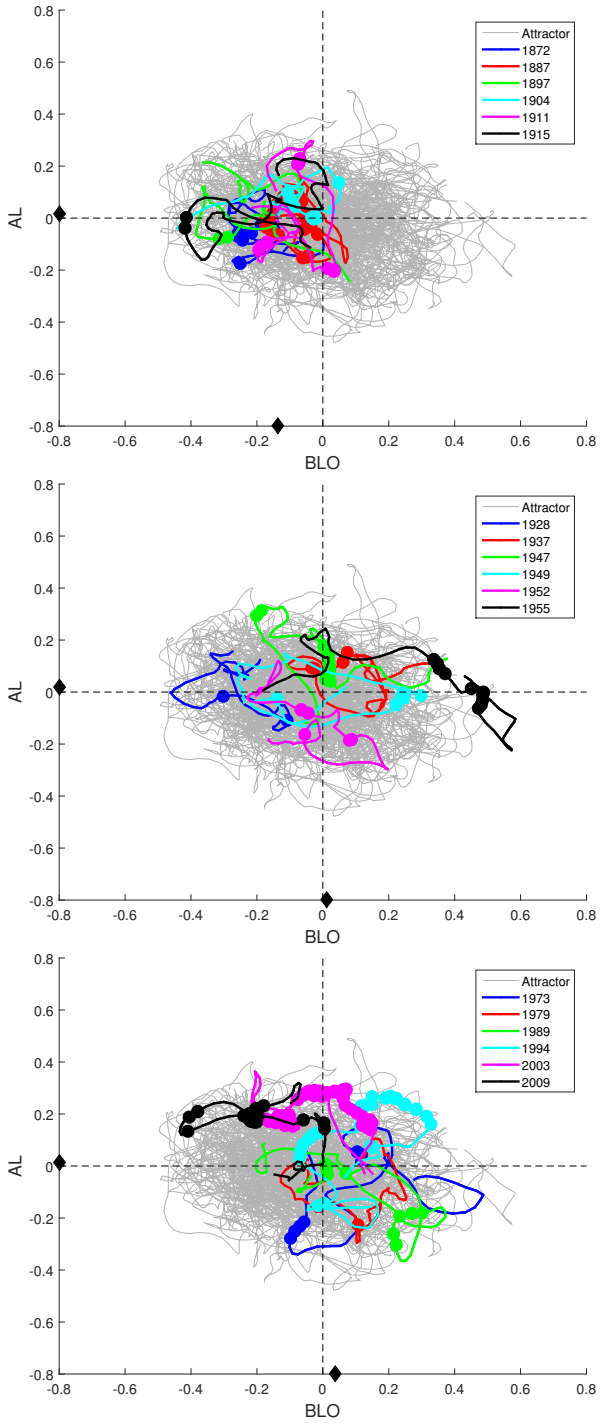


**Figure 4. Dynamical representation of the warmest summers (same method as fig.2a-c in main text) for 20CR during 1871-2011.** Correlations of daily SLP fields and BLO (x-axis), AL (y-axis) weather regimes for three different periods. Warmest summers are colored as in the legend, light grey lines represent all data. Big circles represent days with temperature above the 85th percentile. Average correlations of warmest summers with respect to each weather regime (black circle on x-axis).

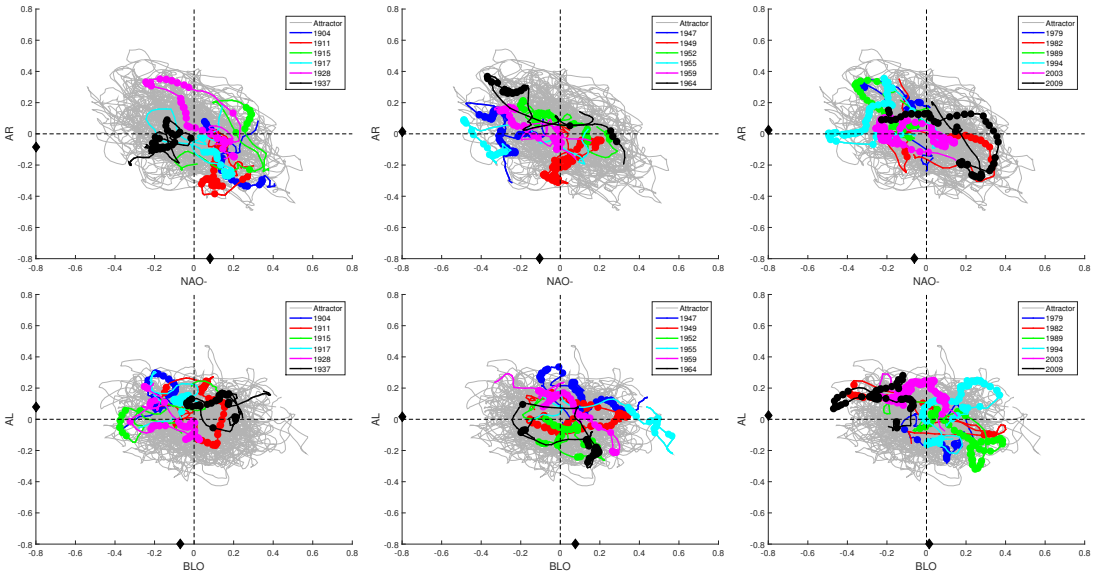


**Figure 5. Dynamical representation of the warmest summers (same as fig.2a-c in main text) for ERA20C during 1900-2010.** Correlations of daily SLP fields and NAO- (x-axis), AR (y-axis) weather regimes in upper panels and correlations of daily SLP fields and BLO (x-axis), AL (y-axis) weather regimes in the bottom panels for three different periods. Warmest summers are colored as in the legend, light grey lines represent all data. Big circles represent days with temperature above 85th percentile. Average correlations of warmest summers with respect to each weather regime (black circle on x-axis).

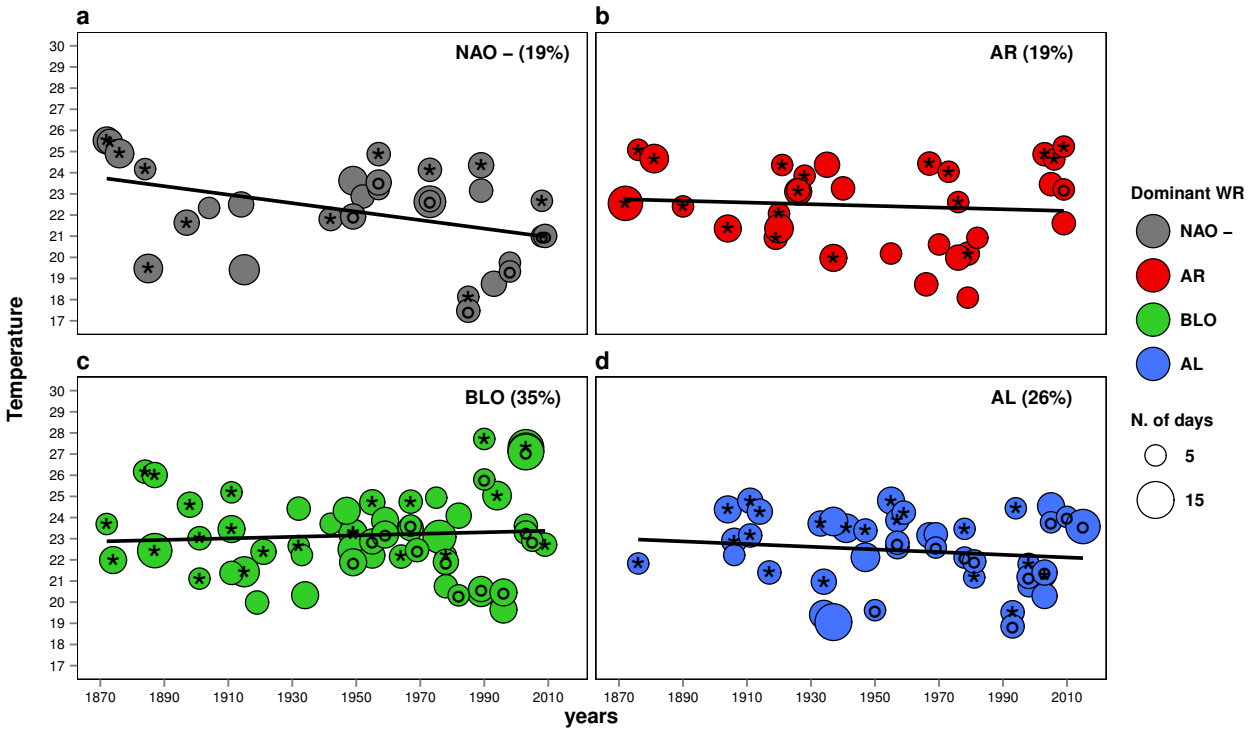


**Figure 6. Dominant weather regimes during Summer Heatwave events in Western-Europe.** Summer heatwave events (P90th Percentile) from 1871 to 2015 for different reanalysis products: 20CR (circle with stars), ERA20C (empty circle), and NCEP (circles with inner circle). Colors correspond to the dominant Weather regime (**a-d,**) in each event, temperature (y-axis) and years (x-axis). Circle sizes depend on the event duration by number of days, the larger the longer duration. Percentages show the frequency of each weather regime. Linear fits are shown in black solid lines.

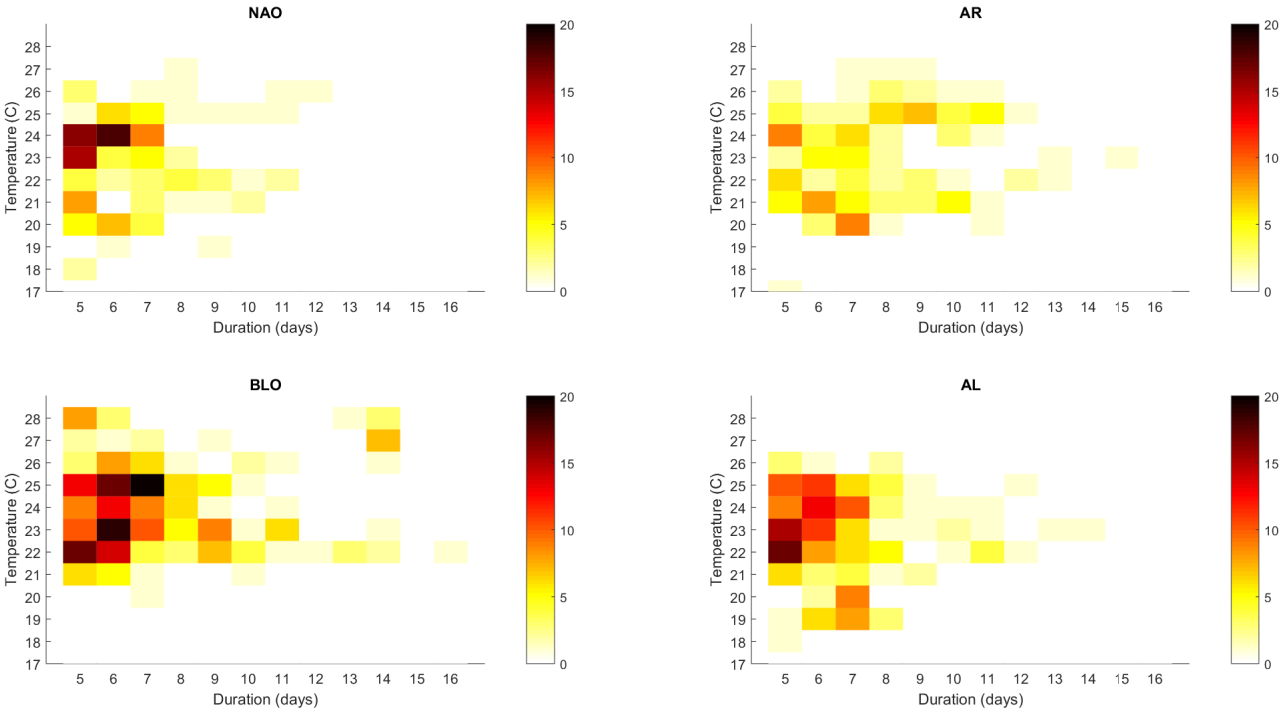


**Figure 7. Density plot of heatwave events**. Temperature (y-axis) vs numbers of days (x-axis) during each heatwave event for the 20CR Ensemble Mean (1871-2011) weather regimes. Colors represent the number of hetwaves events.

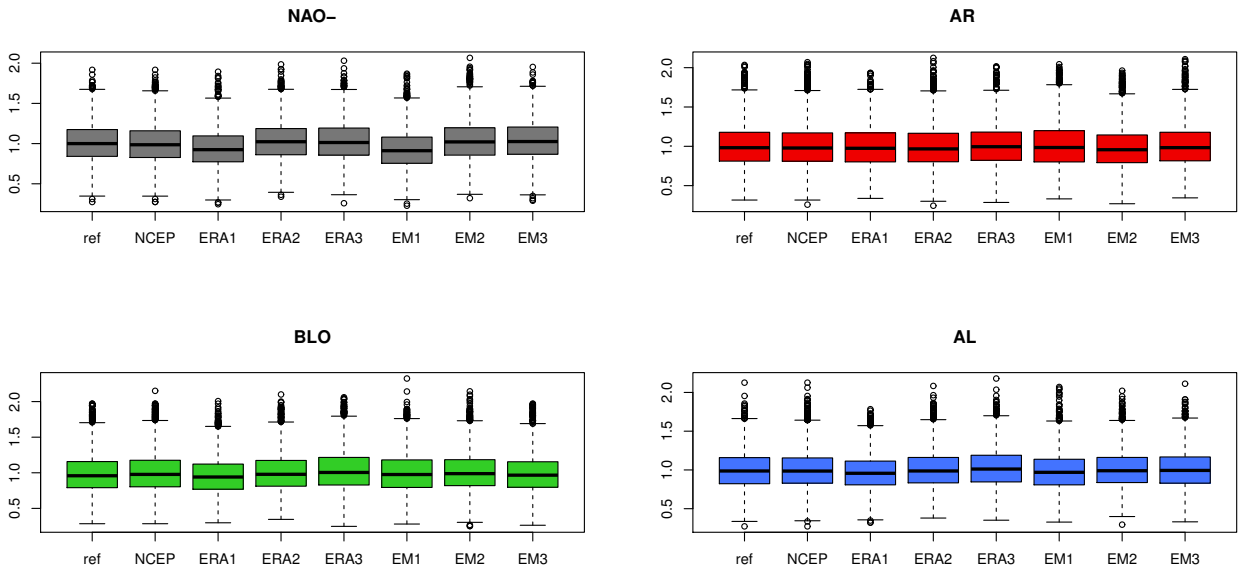


**Figure 8. Boxplots of Absolute Root Mean Square Error by period and weather regime**. Colors represent each weather regime. (See also Table S1).

| $Abs_{RMSE}$ | **Period** | **NAO-** | **AR** | **BLO** | **AL** |
|---|---|---|---|---|---|
| **NCEP** | **(1970-2010)** | **1.01** | **1.00** | **0.98** | **0.99** |
| | (1948-2015) | 1.01 | 1.0 | 1.01 | 1.00 |
| **ERA 20C** | (1900-1936) | 0.95 | 0.99 | 0.96 | 0.97 |
| | (1937-1973) | 1.03 | 0.99 | 1.01 | 1.01 |
| | (1974-2010) | 1.03 | 1.01 | 1.03 | 1.03 |
| **20CR** | (1871-1917) | 0.94 | 1.01 | 1.00 | 0.99 |
| | (1918-1964) | 1.03 | 0.98 | 1.02 | 1.01 |
| | (1965-2011) | 1.04 | 1.01 | 0.99 | 1.01 |

**Table 1. Absolute error of the Root mean square deviation ($Abs_{RMSE}$) of the truncated EOFs during the training period( NCEP:1970-2010) by Weather Regimes** during summer in Western-Europe (see also Figure S8)

| p-value | NAO- | AR | BLO | AL |
|---|---|---|---|---|
| **M0** | 0.42 | 0.56 | 0.20 | 0.23 |
| **M1** | 0.57 | 0.53 | 0.23 | 0.32 |
| **M2** | 0.67 | 0.82 | 0.07 | 0.80 |
| **M3** | 0.88 | 0.74 | 0.09 | 0.87 |
| **M4** | 0.65 | 0.94 | 0.13 | 0.79 |
| **M5** | 0.81 | 0.91 | 0.09 | 0.54 |
| **M6** | 0.29 | 0.84 | 0.27 | 1.00 |
| **M7** | 0.18 | 0.53 | 0.30 | 0.80 |
| **M8** | 0.38 | 0.47 | 0.05 | 0.57 |
| **M9** | 0.71 | 0.63 | 0.45 | 0.81 |
| **EM 20CR** | 0.40 | 0.44 | 0.23 | 0.25 |
| **ERA 20C** | 0.32 | 0.37 | 0.30 | 0.65 |
| **NCEP** | 0.26 | 0.00 | 0.50 | 0.24 |
| **Mean 20C** | 0.54 | 0.67 | 0.19 | 0.63 |
| **Mean rea.** | 0.33 | 0.27 | 0.34 | 0.38 |

**Table 2. p-values of Heatwave events** calculate for each dataset and regime. Mean 20C is the mean of all the members with EM20CR (trend line in figure 3) and Mean rean. is the mean of all the reanalyses (EM20CR, ERA20C, NCEP) (trend line in figure S6). To calculate the p-values we fit a linear model. The null hypothesis is that there is no trend. The statistics and the degrees of freedom are evaluated as in Chamber, 1992 and Wilkinson an Rogers, 1973)

| **Periods** | **NAO-** | **AR** | **BLO** | **AL** |
|---|---|---|---|---|
| Period 1 (30-days filter) | 0.22 | -0.1 | -0.14 | 0.02 |
| Period 2 (30-days filter) | -0.07 | 0.04 | 0.01 | 0.02 |
| Period 3 (30-days filter) | -0.11 | 0.07 | 0.04 | 0.01 |
| Period 1 (Without filter) | 0.23 | -0.11 | -0.14 | 0.02 |
| Period 2 (Without filter) | -0.08 | 0.01 | 0.05 | 0.03 |
| Period 3 (Without filter) | -0.11 | 0.08 | 0.01 | 0.02 |

**Table 3. Average correlations of hottest summers in figure 2**. The three periods correspond to periods plotted in Fig.2 (NAO-, AR) and Fig. S4. (BLO, AL). The three first periods *30-days filter* show the average correlations of the warmest summers in 20CR plotted in the axis as black diamonds in Fig.2 and Fig. S4., applying a 30-days moving average filter for the warmest summers. The three periods *without filter* show the same information but without applying any filter.